International Journal of Innovative Research in Science and Engineering
Volume 08, Issue 06, 2022
www.ijirse.com
ISSN: 2454-9665

Numerical investigation on the implementation and development of high-performance perovskite solar cells using SCAPS-1D software

M. Suresh Kumar[1*], G. Lenish[1], K.Harshitha[1], K. Sivasagar[1], G, Himaja[1]

[1] *Department of Electronics & Communication Engineering, S V College of Engineering, Tirupati, Andhra Pradesh, India 517507.*

***Corresponding Author**

Address corresponds to **Dr. M. Suresh Kumar, Ph.D.,*

Associate Professor, Department of Electronics & Communication Engineering,

S V College of Engineering, Tirupati, Andhra Pradesh, India 517507.

Email id.: msuri88@gmail.com

Abstract

Recently, lead-free organic-inorganic halide perovskites have become promising materials in the development of next generation solar cells. In this work, the numerical modeling and simulation of a methylammonium germanium iodide ($CH_3NH_3GeI_3$) based solar cells were investigated using SCAPS-1D software. For the first time, the stable inorganic p-type quaternary metal chalcogenides such as $Cu_2ZnSnSe_4$ (CZTSe), Cu_2XSnS_4 (where X = Zn, Fe, Ni, Mn, Ba) were chosen as the buffer layer. The hole transporting properties of these buffer layers were studied and compared by evaluating the photovoltaic performance.

Keywords: *Pb-free Perovskite material, methylammonium germanium iodide, p-type buffer layer, SCAPS-1D*

Introduction

The perovskite solar cells (PSCs) have received enormous attention due to their superior optoelectronic properties of perovskite materials, including long carrier diffusion length, ambipolar charge transports, high absorption coefficients and moderate band gap. Decades of device optimization efforts for lead-based perovskite photovoltaics have led to remarkable advances in device performance, the power conversion efficiency (PCE) of PSCs has jumped from 2.2% to the current champion PCE of 25.2%. However, the instability and toxicity of Pb-perovskite make commercialization of these PSCs difficult. Pb-free perovskite is considered the alternative candidate to effectively overcome these fundamental issues. In typical perovskite solar cell design, apart from the perovskite absorber material it is also essential to select suitable electron transport material (ETM)

ISSN: 2454-9665

and a hole transport material (HTM) to improve the stability and reproducibility of PSCs. In this context our work investigates the numerical analysis on choosing appropriate HTM for methylammonium germanium halide ($CH_3NH_3GeI_3$)-perovskite material.

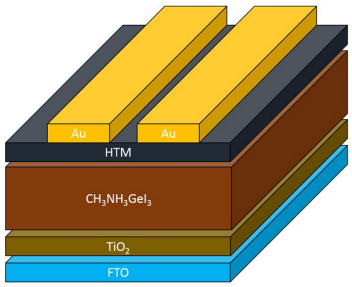

Figure 1: Schematic Structure of the perovskite solar cell.

SCAPS-1D Simulation Methodology

The simulation and the calculations performed out in the SCAPS-1D software is primarily based on three basic equations namely the Poisson's equation, electron continuity equation and hole continuity equation respectively[18,19]. This is a 1D solar cell simulation software that has been developed at the department of Electronics and Information Systems (ELIS) of the University of Gent, Belgium[20]. In this software, the designed model can simulate a maximum of seven semi-conductor layers and besides this, it gives the flexibility of grading and tuning different properties as in energy bandgap, electron affinity, defects, doping, interfacial properties etc. for each of the layers. The software is feasible for simulating different solar device structures from crystalline, amorphous to even organic and perovskite solar cells. The spectral condition under which the simulation has been performed is AM 1.5G 1 sun spectrum. The properties of each of HTL and the perovskite layer have been varied to achieve an optimized result. The thickness and doping concentration has been differed within a feasible range in order to study the plot type obtained with the changing values. This makes it very simple and quite precise to obtain optimum values of each of the layers, which further helps in obtaining the optimized performing solar cell. This is done for all the P type buffer materials taken into account in this work which helps in understanding the performance and effect of properties for each material. The mathematical equations that are crucial in the numerical simulation analysis are described below. For semiconductors, Poisson's Equation is given by:

$$\frac{d^2\Psi(x)}{dx^2} = \frac{q}{\varepsilon}(n - p + N_A - N_D) \quad \ldots\ldots\ldots (1)$$

Where, ε is the permittivity of the semiconductor, N_A represents the acceptor concentration, N_D is the donor concentration and ψ resembles the electrostatic potential.

Now, the electron and hole continuity equations for a semiconductor are given by:

Electron continuity equation:

$$\frac{\partial J_n(x)}{\partial x} - q\frac{\partial n}{\partial t} = +qR \qquad \text{……..(2)}$$

Hole continuity equation:

$$\frac{\partial J_p(x)}{\partial x} + q\frac{\partial p}{\partial t} = -qR \qquad \text{…....(3)}$$

In the above equations (2) and (3), J_n is the current density for electrons, J_P is symbolic of the current density for holes and R represents the rate of carrier recombination.

Another very essential set of equations is the Drift-Diffusion current relations that are given by the continuity equations shown in (4) and (5). There are two ways in which current is conducted in a semiconductor. First and foremost, diffusion current is produced due to the difference in carrier concentration on either sides of the device (concentration gradient). Secondly, and drift current that is build up due to the drift of minority charge carriers under the electric field.

$$J_n = qn\mu_n E + qD_n\frac{\partial n}{\partial x} \qquad \text{……..(4)}$$

$$J_p = qp\mu_p - qD_p\frac{\partial p}{\partial x} \qquad \text{……...(5)}$$

Where, D_p is the diffusion coefficient for holes and D_n is the diffusion coefficient for electrons. E represents the electric field, q is the quantity of charge, n and p represents the number of electrons and holes. μ_n and μ_p represents the mobility of electron and holes respectively. Other relations that govern the performance parameters are as follows:

In this simulation different P type buffer materials will be used to find out best configuration to achieve higher performances. Major attention is given to optimise different parameters in a way through which we can get a clear insight of device performances. The absorption spectra of the p type buffer materials used in this simulation, are shown in Figure 2, which will help us understand the thickness dependence, optical absorption index (extinction factor) of the material that affects the carrier generation distribution and electrical internal resistance of the film.

Results & Discussion

In order to investigate the impact of various HTMs on device performance of $CH_3NH_3GeI_3$ based perovskite solar cells, numerical modeling was carried out using 1D-SCAPS software. Figure 2 illustrates the J-V characteristics of $CH_3NH_3GeI_3$ perovskite solar cell based on different HTMs.

The SCAPS 1D simulation were performed based on tabulated parameters collected from different theoretical and experimental papers. In a solar cell device, every layer plays a deciding role in the device's performance. The assessment of device's performance will be based on four parameters: open circuit voltage, short circuit current density, fill factor, and efficiency. Different hole transport layers

have been used in the device configuration of FTO/TiO_2/$MAGeI_3$/HTL/Au keeping all the parameters same. The variation aids in observing and studying the performance of the device model with different HTLs so that the best suitable material as HTL can be decided for optimization, followed by further study. Fig. 2 shows the J-V characteristics of the simulated PSC with Copper zinc tin selenide (CZTSe), Copper zinc tin sulfide (CZTS), and zinc substituted CZTS compounds: Copper iron tin sulfide (CFTS), Copper nickel tin sulfide (CNTS), Copper barium tin sulfide (CBTS), Copper Manganese tin sulfide (CMTS). The performance obtained after simulation with different HTLs are shown in Table 1. It can be observed that the device with CBTS results in the highest efficiency of 17.16%. Along with efficiency both V_{OC} and J_{SC} also the highest for CBTS as HTL. Nevertheless, the fill factor with CBTS as HTL is 2nd highest but only 3.07% different from the highest FF. Then the 2nd highest performance is from the device with CNTS as the HTL layer since with this the device achieves the 2nd highest efficiency, V_{OC} and J_{SC}. With CNTS the device achieves the highest fill factor compared with other HTLs. The device with the lowest performance is with CFTS since this device results in the lowest efficiency, fill factor, and V_{OC}. The J_{SC} of the device seems to stay almost the same with varying HTL and this might be due to the almost similar absorption coefficient of all the HTLs. With other three HTLs V_{OC}, J_{SC} and efficiency are almost equal. An attempt will be made to explain the reason for the results corresponding to the devices with highest and lowest performance.

The Built-in potential displayed in table 1 is calculated from the band structures by measuring the separation between the Fermi levels at the distance where the first discontinuity takes place. It can be noticed from table 1 that with CBTS the built-in potential (V_{bi}) is 1.29V and this happens to be the highest among all the V_{bi} obtained. This is the reason why with this material the device achieves the highest V_{OC} and efficiency. V_{OC} is an indication of the amount of recombination in the device. As the V_{bi} increases the separation of the generated exciton will be effective and hence reduces the recombination rate, which leads to improved V_{oc}. Therefore with increasing V_{bi} the V_{OC} increases. Due to the effective separation of photogenerated charges the efficiency also increases. The Device with CFTS achieves the lowest performance and the reason for this is due to the small V_{bi}. This leads to ineffective charge separation and leads to low V_{OC} and efficiency. Another reason for this low performance is because with this material the valence energy level takes the largest jump in the discontinuity region between absorber and the HTL. This high energy difference hinders the flow of the holes into the HTL [22]. Therefore one must keep in mind while selecting a HTL material that this energy difference must be moderate. Due to the astounding device performance with CBTS, this material is chosen as the most suitable HTL for the lead free perovksite solar cell.

Table 1: Device performance with all HTL

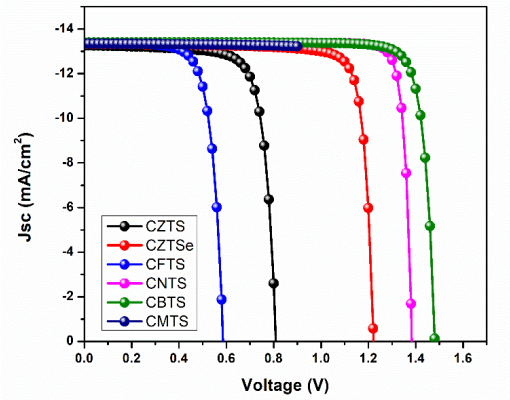

Figure 2: J-V curve of device with varying HTL.

HTL	Absorbing material	Voc (V)	Jsc (mA/cm^2)	FF (%)	Efficiency (%)
CZTS	$CH_3NH_3GeI_3$	0.809	13.265	77.56	8.33
CZTSe		1.221	13.338	84.67	13.80
CFTS		0.586	13.390	74.08	5.82
CNTS		1.3837	13.397	89.58	16.61
CBTS		1.480	13.398	86.51	17.16
CMTS		0.8108	13.266	77.41	8.33

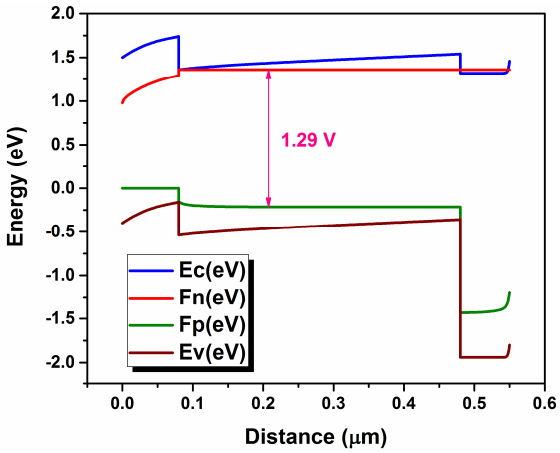

Figure 3: Band diagram of the device with CBTS as the HTL

Constructing an optimized device in a lab is very tedious job due to the task being trial and error based in nature. Through SCAPS 1D its possible to obtain the optimized device parameters without going through a heavily laborious work. Yet there remain a question of reproducibility of the simulated results, due to the existence of defect densities. Nevertheless, it gives the researchers a starting point from which they can begin executing their optimization protocol. The absorber layer has significant influence on the device performance due to most of the charges being photogenerated in this layer. Fig. 4 shows the various plots depicting the variation of performance parameters with varying absorber layer thickness from 100 nm to 1000 nm by keeping the other parameters same. It can be observed how open circuit voltage varies reciprocally with short circuit current. The reason for this behavior is as follows. The open circuit voltage of a solar cell device is governed by the equation [23]:

$$V_{oc} = \frac{nKT}{e} \ln\left(\frac{Jsc}{J_0} + 1\right) \quad \ldots\ldots (6)$$

Where $\frac{nKT}{e}$ is the thermal velocity and the J_0 being the dark saturation current. J_0 is highly dependent on the amount of recombinations in the device [23] and it is evident from the equation that V_{oc} decreases with increasing J_0. Therefore the decrease in V_{OC} with increasing absorber thickness is justified with increase in recombination rate. J_{SC} on the other hand increases, as mentioned before, with increasing absorber thickness and then it seems to saturate for larger thicknesses. A thin absorber is incapable of absorbing long wavelength photons [24], resulting in partial absorption of light and therefore low exciton generation. With increasing absorber thickness photons with all wavelengths will be absorber, resulting in an improved exciton generation amount, which leads to an increasing J_{SC}. Nevertheless, for thickness exceeding the absorption coefficient of corresponding wavelengths all of the light will be absorbed and therefore results in a stagnant Jsc with increasing thickness. The fill factor seems to decrease with increasing thickness. As the absorber thickness increases the series resistance increases, which results in the fill factor to decrease. The efficiency on the other hand behaves in the same way J_{SC} behaves with increasing absorber thickness and the justification for this trend is the same one given to explain J_{SC} trend. Around 900 nm the efficiency starts to saturate and therefore this was chosen as the optimized absorber layer thickness.

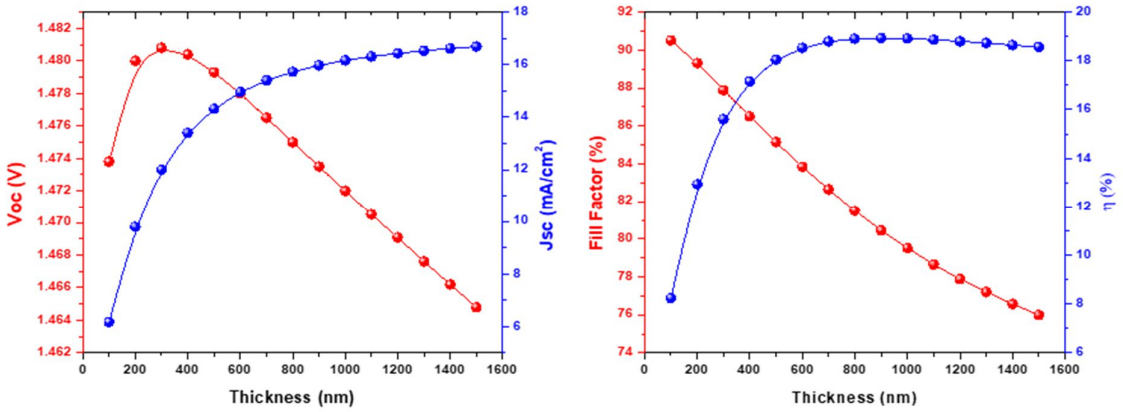

Figure 4: Device performance with varying absorber thickness

Doping levels in a material can influence the material's conductivity and the recombination rates. So it is very importance to find the optimized doping level in the absorber layer. According to the tabulated parameter for the device simulation $CH_3NH_3GeI_3$ has equal donor and acceptor concentration, which means that the material is an intrinsic semiconductor. Yet the material is slightly p-type in room temperature [23]. So the acceptor (instead of donor) doping concentration was varied from 1×10^8 cm^{-3} to 1×10^{17} cm^{-3} to find the optimum doping concentration. Fig. 5 shows how the device performance varies with acceptor doping concentration. The mentioned doping concentration range was chosen in such a way as to avoid auger recombination, which can have dominating influence on device performance for higher doping concentrations (>1.00E+018 cm^{-3}) [24]. From Fig. 5 it can be inferred that the device performance changes drastically after an acceptor concentration of $1 \times 10^{14} cm^{-3}$. The V_{OC} of the device sees an increase because the built in potential across the device increases with increasing doping concentration [24], which leads to effective separation and transportation of the photogenerated charges. This in effect leads to an improved fill factor because the conductivity of the layer increases. Also the efficiency improves due to the effective separation and collection of the generated charges. Despite the decreasing JSC the V_{OC} is increases which means that J_0 is increasing at a rate larger than J_{SC}. The decrease in FF and hence the decrease in efficiency after 1×10^{15} cm^{-3} is due to the creation of more scattering centers which leads to increasing series resistance. The efficiency reaches an optimum value at 1×10^{15} cm^{-3} doping concentration so this is taken as the optimum concentration.

International Journal of Innovative Research in Science and Engineering
Volume 08, Issue 06, 2022
www.ijirse.com
ISSN: 2454-9665

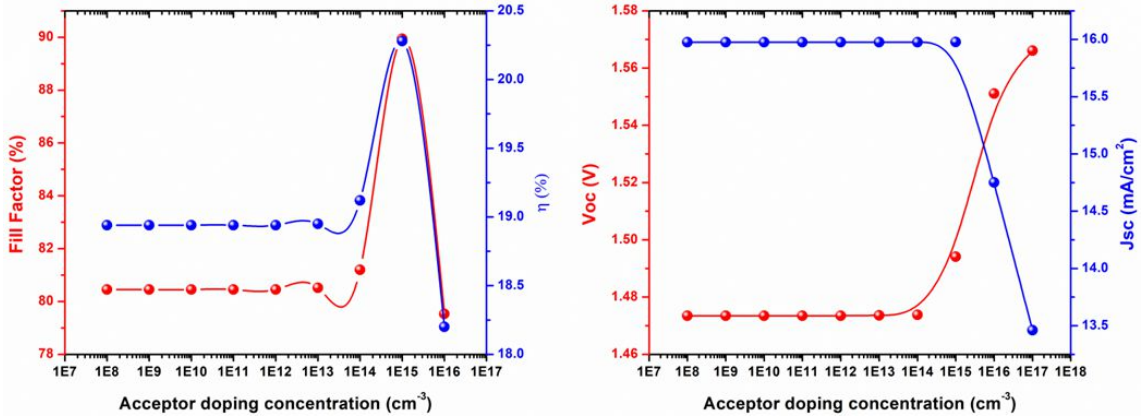

Figure 5: Device performance with varying acceptor doping concentration

Fig. 6 shows how the electrical performance of the device change with varying hole transport layer thickness. This layer plays the role of effectively transporting the holes to the back contact. The hole transport layer thickness was varied from 100 nm to 600 nm. It can be noticed from the figure that the device performance doesn't change much with increasing thickness. Even though the hole transport layer thickness doesn't have much effect on the device performance it is not recommended to take small thicknesses as the optimum thickness. There is a possibility that small thicknesses will be unable to fully cover the protruding perovskite crystals in the absorber layer and this leads to large leakage current. So it is best to chose 200nm as the optimum hole transport layer thickness [26]. In order to understand how the device responds to a varying acceptor doping concentration the doping level was varied from 1×10^{11} cm^{-3} to 1×10^{24} cm^{-3} and the response is shown in Fig. 7. The efficiency of the device seems to increase initially and then starts to saturate after a particular doping level. This increase in efficiency is the due to the improved V_{OC} and fill factor. The level after which the efficiency saturates is about 1×10^{20} cm^{3} and this is chosen as the optimized acceptor doping concentration. With this the device optimization is completed with absorber thickness 900 nm, absorber acceptor doping concentration 1×10^{15} cm^{-3}, HTL thickness 200 nm, HTL acceptor doping concentration 1×10^{20} cm^{-3}. Fig. 8 shows the J-V curve of the optimized device as well as its performance parameters.

International Journal of Innovative Research in Science and Engineering
Volume 08, Issue 06, 2022
www.ijirse.com
ISSN: 2454-9665

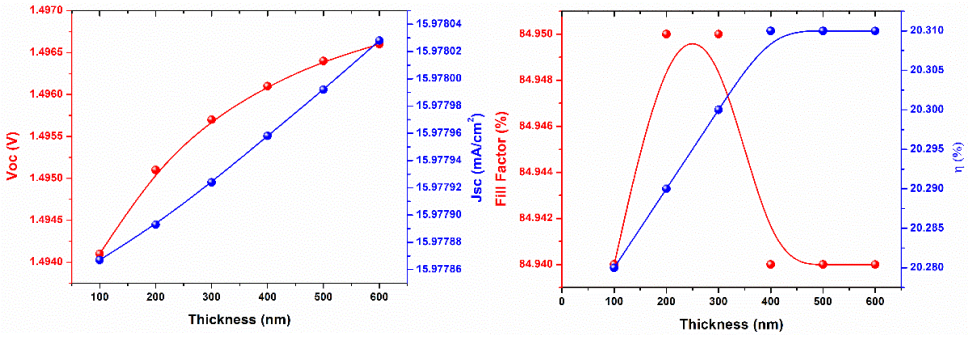

Figure 6: Device performance with varying HTL thickness

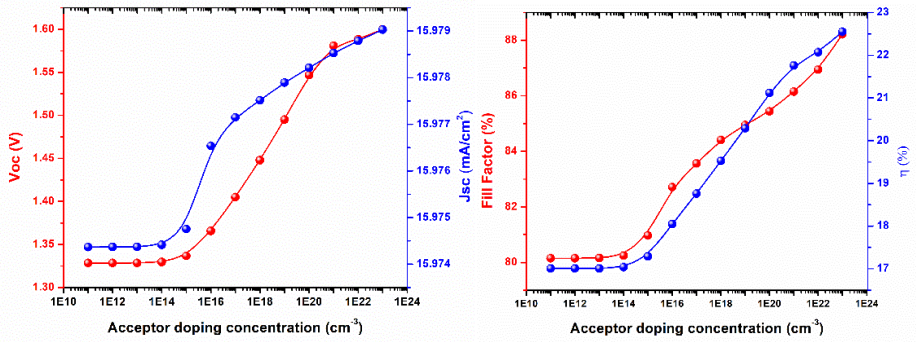

Figure 7: Device performance with varying acceptor doping concentration.

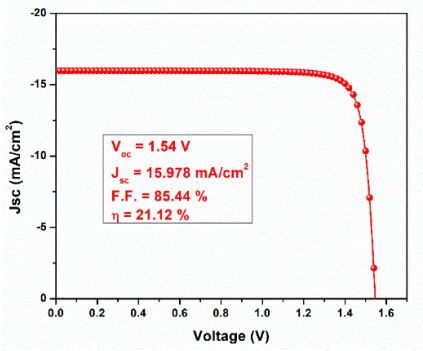

Figure 8: J-V cure for the optimized device with performance parameters

Interface defect density at HTL / absorber interface (ID1) was varied from 1×10^7 cm^{-3} to 1×10^{15} cm^{-3} , keeping other parameters constant and the effects on the device performance is shown in Fig 8. As it can be seen the V_{OC} remains constant and then starts to decrease after $1 \times 10^{10} cm^{-3}$. This is obvious because the defects lead to improved recombination rate and V_{OC} as mentioned before is an indication of the amount of recombinations in the device. Hence V_{OC} falls with increasing defect density. The fill factor starts to decrease after 1×10^{12} cm^{-3} and this decrease is due to the addition of

series resistance in the device. The efficiency seems to remain constant and then starts to decrease after $1 \times 10^{11} cm^{-3}$. This decrease in efficiency is due to the fall in V_{OC} and fill factor. Therefore the device can tolerate defects density up to $1 \times 10^{11} cm^{-3}$ and beyond this the device seems to perform with falling efficiency.

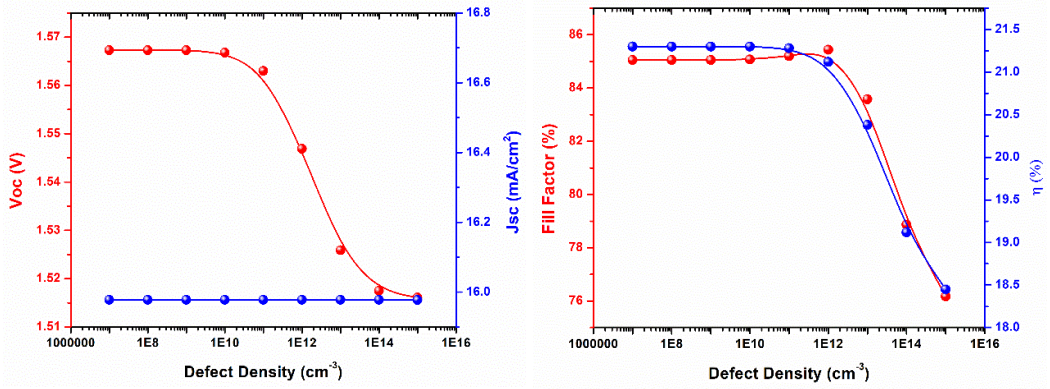

Figure 9: Device performance with varying ID1

Interface defect density at absorber / ETL interface (ID2) was varied from 1×10^{7} cm^{-3} to 1×10^{15} cm^{-3} , keeping other parameters constant and the effects on the deice performance is shown in Fig 10. The trend in variation of all the performance parameters is the same as that seen for the defect density variation in ID1 except for the J_{SC} variation. It can be noticed that the tolerance limit is 1×10^{10} cm^{-3}, which is ten times less than the tolerance limit in ID_1. Therefore, defects in ID_2 have more impact on the device performance than that in ID_1. The absorber defect density was varied from 1×10^{13} cm^{-3} to 1×10^{20} cm^{-3} , keeping other parameters constant and the effects on the device performance is shown in Fig 11. The V_{OC} remains constant for small defect densities but after 1×10^{17} cm^{-3} it starts to decrease. The reason, as usual, is due to the defect densities acting as recombination and scattering centers which leads to an increase in recombination rate. The J_{SC} also follows the same trend but it can be noticed that the defects have more impact on it than on the V_{OC}. The reason for the decrease is again due to the increase in recombination rate. The same reason also applies for the falling fill factor and efficiency. The defect density after which the efficiency starts to fall is after 1×10^{13} cm^{-3} and therefore this is taken as the device's tolerance limit. Beyond this limit the device starts to perform with lower efficiency.

International Journal of Innovative Research in Science and Engineering
Volume 08, Issue 06, 2022
www.ijirse.com
ISSN: 2454-9665

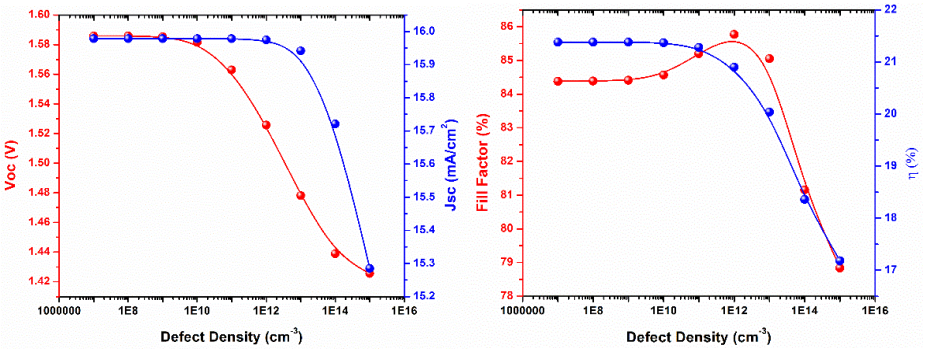

Figure 10: Device performance with varying ID2

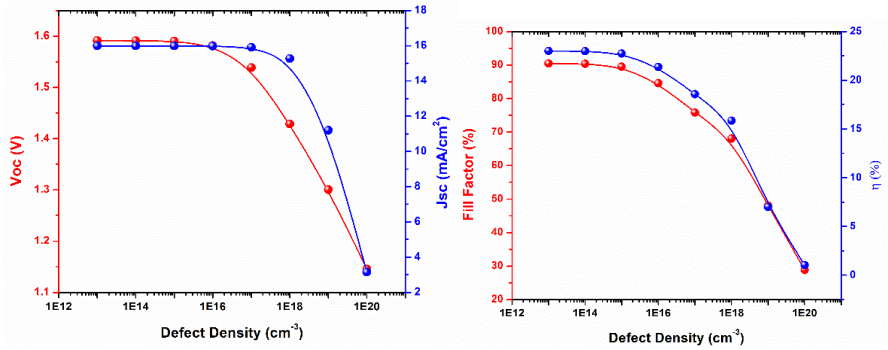

Figure 11: Device performance with varying absorber defect density

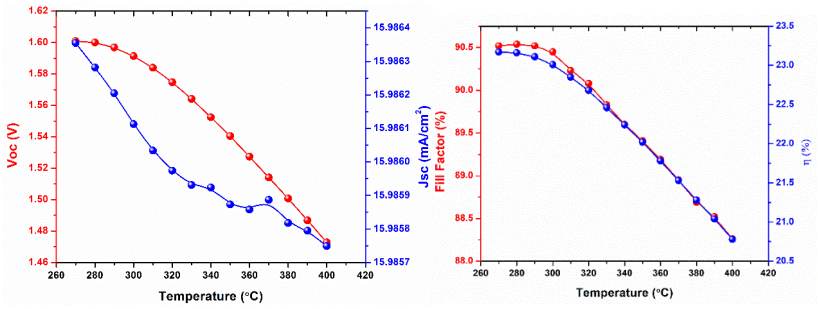

Figure 12: Device performance with varying temperature

The effect of the temperature on the optimized solar cell device performance will be studied by varying the temperature of the system from 270 K to 400 K. A typical solar module converts 6-20% of the incident light into electricity and the rest of the light goes into heating the solar module [30]. Therefore, in outdoor conditions the solar cell device is operating at a temperature higher that 25^0C. So it import to understand the temperature's effect on the device performance. Fig 12 shows how the four performance parameters vary with varying temperature from 270 K to 400 K. It can be notice

ISSN: 2454-9665

from the figure that the four parameters decline with increasing temperature. The least affected is the device's J_{SC} since it is evident from the figure that the declination is very small (almost constant). This solar cell's behavior with varying temperature can be explained. At higher temperatures the band gap of the material usually decreases [31] and as a consequence of this diminished band gap the device can start absorbing longer wavelength photons. Therefore, more carriers will be photogenerated and this leads to an improvement in device's J_{SC}. Ironically the simulation result shows the opposite. The reason for this trend is as follows. Resistivity in a semiconductor is inversely proportional to the product of carrier concentration and the mobility of the charge carriers. It is true that in an extrinsic semiconductor, as the temperature increases more electrons gets excited to the conduction band, thus increasing the conductivity and decreasing the resistivity of the material. While the concentration increases the mobility of the charge carriers on the other hand will decline because the materials used in this device are highly doped. Therefore, as the temperature increases the scattering also increases due to the existence of the doped ions (which act as scattering centers). Also with increasing temperature the lattice vibration also increases, in other words more phonon are generate, which will only aid in more scattering. This all leads to the mobility to decrease, which increases the device's resistivity and hence the J_{SC} decreases. From the simulated data it is clear that the mobility decreases at a faster rate than the carrier concentration rate. This might be the only explanation for the J_{SC} decreasing trend. It is evident from Fig 12 that in spite of the almost constant trend of J_{SC} with increasing temperature the Voc decreases at a significant rate. The reason for this is that the saturation current increases with increase in temperature [31] and this leads to the decrease in V_{OC} according to equation1. As the saturation current increases the recombination rate also increases. This is the reason for the V_{OC} decreasing trend and hence responsible for the declining trend of fill factor and efficiency. From this discussion is recommend therefore to operate the device in room temperature conditions to prevent the device from underperforming.

Conclusion

In this work $CH_3NH_3GeI_3$ based solar cell device was simulated with different HTLs, then the best HTL was chosen to optimize and to study the effect of defect densities as well as temperature on the device's performance. The efficiency of the optimized device was 21.12% with absorber thickness 900 nm, absorber acceptor doping concentration 1×10^{15} cm^{-3}, HTL thickness 200 nm, HTL acceptor doping concentration 1×10^{20} cm^{-3}. The device performance starts deteriorating when ID1, ID2, and absorber defect densities cross beyond 1×10^{11} , 1×10^{10} , and 1×10^{13} respectively. The temperature has a negative effect on the device's performance therefore it is recommended to operate the device under room temperature.

References

[1] Singh, Neelima, Alpana Agarwal, and Mohit Agarwal. "Numerical simulation of highly efficient lead-free all-perovskite tandem solar cell." Solar Energy 208 (2020): 399-410.

[2] Yoshikawa, Kunta, et al. "Silicon heterojunction solar cell with interdigitated back contacts for a photoconversion efficiency over 26%." Nature energy 2.5 (2017): 1-8.

[3] Richter, Armin, Martin Hermle, and Stefan W. Glunz. "Reassessment of the limiting efficiency for crystalline silicon solar cells." IEEE journal of photovoltaics 3.4 (2013): 1184-1191.

[4] Shah, A. V., R. Platz, and Herbert Keppner. "Thin-film silicon solar cells: a review and selected trends." Solar energy materials and solar cells 38.1-4 (1995): 501-520.

[5] Günes, Serap, and Niyazi Serdar Sariciftci. "Hybrid solar cells." Inorganica Chimica Acta 361.3 (2008): 581-588.

[6] Sharma, Divya, Rajesh Mehra, and Balwinder Raj. "Design and Analysis of Various Solar Cell Technologies for Improvements in Efficiencies: A Review." (2021).

[7] Imamzai, Mohammadnoor, et al. "A review on comparison between traditional silicon solar cells and thin-film CdTe solar cells." Proceedings of National Graduate Conference (Nat-Grad. 2012.

[8] Beaucarne, Guy. "Silicon thin-film solar cells." Advances in OptoElectronics 2007 (2007).

[9] Schileo, Giorgio, and Giulia Grancini. "Lead or no lead? Availability, toxicity, sustainability and environmental impact of lead-free perovskite solar cells." Journal of Materials Chemistry C 9.1 (2021): 67-76.

[10] Wang, Minghao, et al. "Lead-free perovskite materials for solar cells." Nano-Micro Letters 13.1 (2021): 1-36.

[11] Kumar, Naveen, Jyoti Rani, and Rajnish Kurchania. "A review on power conversion efficiency of lead iodide perovskite-based solar cells." Materials Today: Proceedings (2020).

[12] Smith, Ian C., et al. "A layered hybrid perovskite solar-cell absorber with enhanced moisture stability." Angewandte Chemie 126.42 (2014): 11414-11417.

[13] Kanoun, Ahmed-Ali, et al. "Toward development of high-performance perovskite solar cells based on CH3NH3GeI3 using computational approach." Solar Energy 182 (2019): 237-244.

[14] Kim, Guan-Woo, et al. "Hole transport materials in conventional structural (n–i–p) perovskite solar cells: from past to the future." Advanced Energy Materials 10.8 (2020): 1903403.

[15] Hima, Abdelkader, and Nacereddine Lakhdar. "Enhancement of efficiency and stability of CH3NH3GeI3 solar cells with CuSbS2." Optical Materials 99 (2020): 109607.

[16] Nazligul, Ahmet Sencer, Mingqing Wang, and Kwang Leong Choy. "Recent development in earth-abundant kesterite materials and their applications." Sustainability 12.12 (2020): 5138.

[17] Wu, Qiliang, et al. "Kesterite Cu2ZnSnS4 as a low-cost inorganic hole-transporting material for high-efficiency perovskite solar cells." ACS applied materials & interfaces 7.51 (2015): 28466-28473.

[18] Dridi, S., N. Bitri, and M. Abaab. "Synthesis of quaternary Cu2NiSnS4 thin films as a solar energy material prepared through «Spray» technique." Materials Letters 204 (2017): 61-64.

[19] Wibowo, Rachmat Adhi, et al. "Single step preparation of quaternary Cu2ZnSnSe4 thin films by RF magnetron sputtering from binary chalcogenide targets." Journal of Physics and Chemistry of Solids 68.10 (2007): 1908-1913.

[20] Souli, Mehdi, et al. "Physical properties evolution of sprayed Cu2MgSnS4 thin films with growth parameters and vacuum annealing." Superlattices and Microstructures 147 (2020): 106711.

[21] Chen, Zhu, et al. "Solution-processed trigonal Cu2BaSnS4 thin-film solar cells." ACS Applied Energy Materials 1.7 (2018): 3420-3427.

[22] Khattak, Yousaf Hameed, et al. "CZTSe Kesterite as an Alternative Hole Transport Layer for MASnI 3 Perovskite Solar Cells." Journal of Electronic Materials 48.9 (2019): 5723-5733.

[23] Kanoun, Ahmed-Ali, et al. "Toward development of high-performance perovskite solar cells based on CH3NH3GeI3 using computational approach." Solar Energy 182 (2019): 237-244.

[24] Bag, Atanu, et al. "Effect of absorber layer, hole transport layer thicknesses, and its doping density on the performance of perovskite solar cells by device simulation." Solar Energy 196 (2020): 177-182.

[25] Zhao, Yu-Qing, et al. "Tuning charge carrier types, superior mobility and absorption in lead-free perovskite CH3NH3GeI3: theoretical study." Electrochimica Acta 247 (2017): 891-898.

[26] Kopacic, Indira, et al. "Enhanced performance of germanium halide perovskite solar cells through compositional engineering." ACS Applied Energy Materials 1.2 (2018): 343-347.

[27] Mandadapu, Usha, S. Victor Vedanayakam, and K. Thyagarajan. "Simulation and analysis of lead based perovskite solar cell using SCAPS-1D." Indian Journal of Science and Technology 10.11 (2017): 65-72.

[28] Qiu, Longbin, Luis K. Ono, and Yabing Qi. "Advances and challenges to the commercialization of organic–inorganic halide perovskite solar cell technology." Materials today energy 7 (2018): 169-189.

[29] Chouhan, Arun Singh, Naga Prathibha Jasti, and Sushobhan Avasthi. "Effect of interface defect density on performance of perovskite solar cell: Correlation of simulation and experiment." Materials Letters 221 (2018): 150-153.

[30] Dubey, Swapnil, Jatin Narotam Sarvaiya, and Bharath Seshadri. "Temperature dependent photovoltaic (PV) efficiency and its effect on PV production in the world–a review." Energy Procedia 33 (2013): 311-321.

[31] Meyer, Edson L., and E. Ernest Van Dyk. "Assessing the reliability and degradation of photovoltaic module performance parameters." IEEE Transactions on reliability 53.1 (2004): 83-92.

[32] Jena, Madhab Chandra. "Optimization of solar power generation efficiency using MINITAB

ISSN: 2454-9665

software." International Journal in IT & Engineering 3.2 (2015): 23-47.

[33] Entner, Robert. Modeling and simulation of negative bias temperature instability. Diss. 2007.

[34] Singh, Anand Kumar, et al. "Performance optimization of lead free-MASnI3 based solar cell with 27% efficiency by numerical simulation." Optical Materials 117 (2021): 111193.